*Geophys. J. Int.* (1998) **135,** 255–263

# Traveltimes for infrasonic waves propagating in a stratified atmosphere

Milton A. Garcés,* Roger A. Hansen and Kent G. Lindquist
*Geophysical Institute, University of Alaska, Fairbanks, Alaska, USA*

Accepted 1998 April 14. Received 1998 April 9; in original form 1997 April 10

## SUMMARY

The tau–*p* method of Buland & Chapman (1983) is reformulated for sound waves propagating in a stratified atmosphere under the influence of a height-dependent wind velocity profile. For a given launch angle along a specified azimuth, the ray parameter is redefined to include the influence of the horizontal wind component along the direction of wave propagation. Under the assumption of negligible horizontal wind shear, the horizontal wind component transverse to the ray propagation does not affect the direction of the wave normal, but displaces the reference frame of the moving wavefront, thus altering the observed incidence azimuth. Expressions are derived for the time, horizontal range, and transverse range of the arriving waves as a function of ray parameter. Algorithms for the location of infrasonic wave sources using the modified tau–*p* formulation in conjunction with regional atmospheric wind and temperature data are discussed.

**Key words:** array, atmosphere, guided waves, infrasound, traveltime, wave propagation.

## INTRODUCTION

The arrival times of pressure waves recorded by pressure sensors and infrasonic arrays permit the location of explosive sources detonated in the atmosphere. However, the determination of traveltimes in a stratified atmosphere differs from the traveltime determination in the solid Earth in that there is significant spatial and temporal variability in the physical properties of the atmosphere. For the purposes of traveltime determination, the principal parameters of interest are the temperature and wind fields. For an initial estimate, the sound speed, $c$ ($\mathrm{ms}^{-1}$), in a quiescent atmosphere can be approximated from the absolute temperature, $\Theta$ (K), by using the relationship

$$c = \sqrt{\gamma_g r \Theta}, \tag{1}$$

where $\gamma_g$ is the ratio of specific heats and $r$ is the gas constant for air. Throughout this paper, we will use the value $\gamma_g r = 402.8\ \mathrm{m^2\ s^{-2}\ K^{-1}}$ (Diamond 1963). A more sophisticated relationship may be utilized for the sound speed as a function of the chemical composition, temperature, pressure, and humidity of the atmosphere (Cramer 1992), but the estimate provided by eq. (1) has the advantage of requiring a minimum of input data. Fig. 1(a) shows a typical sound-speed profile in the atmosphere, obtained from eq. (1) using the temperature profile for a typical atmosphere in December at a latitude of 40°N (Houghton 1986). In the absence of clouds (above the troposphere), the absorption of solar radiation in the atmosphere determines the temperature profile (Beer 1975). Above 100 km, short-wavelength radiation is absorbed by molecular oxygen; between 35 and 70 km, ultraviolet radiation is absorbed by ozone, and infrared energy is emitted by carbon dioxide; in the lower 15 km, water vapour and carbon dioxide absorb infrared energy reflected by the Earth; and at ground level, land and sea surfaces absorb visible radiation (Houghton 1986; Beer 1975). Following the sound-speed profile of Fig. 1, which mimics the temperature profile (eq. 1), the atmosphere is divided into distinct regions, the lowest being the troposphere, where the temperature decreases with height. The tropopause (7–17 km), identified by a marked increase in static stability, indicates the transition into the stratosphere, where temperature increases up to the stratopause (45–55) km. The temperature then decreases with height in the mesosphere until the mesopause is reached, at an elevation of 80–85 km. In the overlying thermosphere, temperature increases up to a height of approximately 200 km, and then generally remains constant because of the high thermal conductivity of the neutral gas, which promotes rapid downward energy transfer. The temperature profile above 200 km will be significantly altered by solar activity, as increased activity may increase the thermospheric temperature and modify the high-altitude profile (Beer 1974). The sound-speed profile will be modified by seasonal and daily fluctuations in the atmospheric temperature (Donn & Rind 1971), which may be obtained from satellite data (Hervig *et al.*

* Now at: Aso Volcanological Laboratory, Kyoto University, Choyo-son, Aso-gun, Kumamoto 869-1400, Japan.
E-mail: milton@aso.kugi.kyoto-u.ac.jp

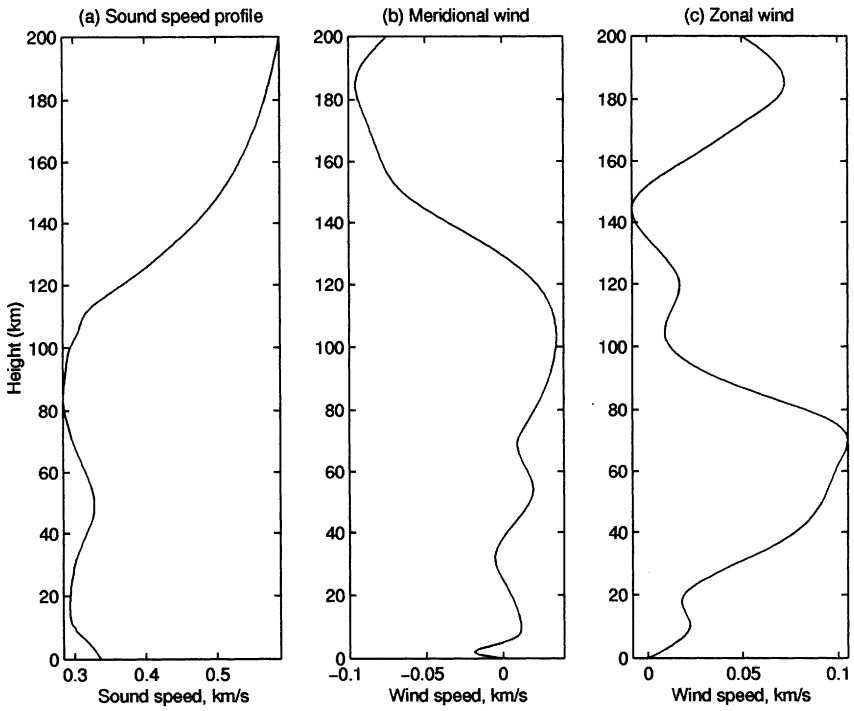


**Figure 1.** (a) Sound speed (km s$^{-1}$) as a function of altitude (km) for a typical atmosphere in December at a latitude of 40°N (Houghton 1986). Characteristic zonal (E–W, panel b), and meridional (N–S, panel c) wind profiles are shown for a mid-latitude region. N and E components are given by positive values.

1996; Hedin *et al.* 1996). As will be seen later in the text, most of the downward propagating acoustic energy observed at the Earth's surface is a consequence of refraction from the thermosphere and the stratopause, where the sound speed increases with elevation, and from the troposphere, where the westerly winds increase with height.

Wind fields vary spatially, seasonally, and diurnally (Donn & Rind 1971; Georges & Beasly 1977), and may dramatically affect the spatial distribution of the sound field. With the recent availability of high-altitude wind magnitude and direction data from the Upper Atmosphere Research Satellite (UARS), the possibility of constructing accurate time-dependent infrasonic wave propagation models in the atmosphere has become feasible (Fleming *et al.* 1996). Characteristic winter zonal (E–W) and meridional (N–S) wind profiles for mid-latitude regions are shown in Figs 1(b) and (c). These profiles have been modified from those of Georges & Beasly (1977) for heights below 10 km, and the justification for these modifications are given below. Note the high zonal wind velocity in the mesophere, where the sound speed reaches its lowest value. The addition of the wind field introduces anisotropy in the infrasonic wave propagation problem, and significantly alters the propagating branches in the traveltime plots, as will be seen in the next section. The high meridional winds in the thermosphere (Fig. 1b) will cause less anisotropy in the infrasonic wave propagation medium than the zonal winds in the mesosphere because of the larger sound-speed values at high elevations. Below 10 km, the zonal wind profile of Georges & Beasley (1977) shows a decreasing westerly wind with height, which is a trend that is not often observed. A more characteristic zonal wind profile (ReVelle, personal communication, 1997) has been used for the first 10 km, and is shown in Fig. 1. In addition, the meridional wind is assumed to be zero at the Earth's surface (Donn & Rind 1971), and to increase to a northerly wind speed of 15 m s$^{-1}$ at 1 km height. These modifications have produced traveltime branches for tropopause ducted waves, which would be absent if the wind profiles of Georges & Beasly (1977) were used.

This paper demonstrates that it is possible to average over space and time to produce regional atmospheric sound-speed models if the wave propagation models are coupled into meteorological databases that provide temperature and wind speeds up to a height of 150–200 km over selected locations. Once a source of infrasonic waves is detected using infrasonic arrays, the first step would be to estimate the source location using triangulation or intersecting array beams. With a known preliminary source location, the average temperature and wind profile as a function of altitude can be computed from meteorological data for that region. Further iterations will be performed with these improved models, using as many arriving phases as can be identified, until the optimum solution is found. This manuscript lays the theoretical foundation to implement the tau–$p$ method of Buland & Chapman (1983) for the determination of traveltime curves in a moving atmosphere, with the aim of providing improved source-location algorithms for infrasonic waves.

## RAY TRACING IN A MOVING MEDIUM

To perform ray tracing in a moving medium it is advantageous to adopt two coordinate systems, one corresponding to the

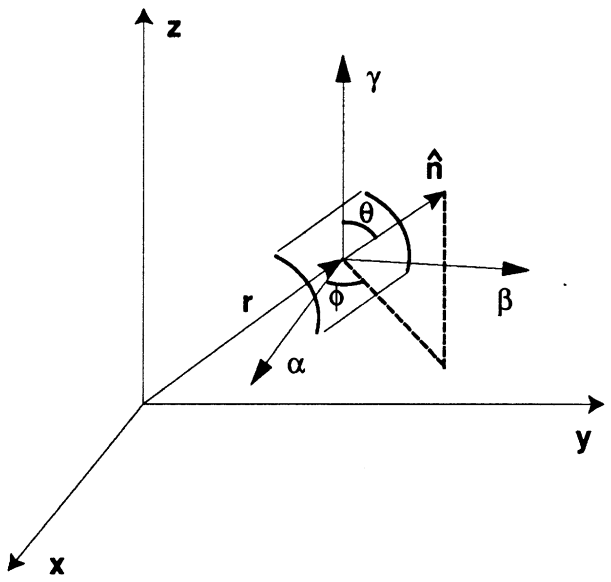


**Figure 2.** Rectangular coordinate system, where $\hat{\mathbf{n}}$ is the unit normal to the wavefront, which is travelling in a moving reference frame.

stationary observer in the Earth and one that is moving with the acoustic wavefront. Following the approach of Lindsay (1960, pp. 296–298), we use a Cartesian coordinate system, as shown in Fig. 2. The position vector $\mathbf{r}$ goes from the origin of the stationary coordinate system to the origin of the second coordinate system, which is moving with the mean wind, $\mathbf{u}$. The unit vector $\hat{\mathbf{n}}$ marks the normal to the wavefront, which propagates with a sound speed $c$ and travels with the moving coodinate system. The three direction cosines of the wave normal, $\alpha$, $\beta$, and $\gamma$, are shown in Fig. 2.

The rate of change of the position vector, which marks the total distance travelled by the wave, is

$$\frac{d\mathbf{r}}{dt} = c\hat{\mathbf{n}} + \mathbf{u}, \tag{2}$$

and the rate of change of the wave normal is

$$\frac{d\hat{\mathbf{n}}}{dt} = (\hat{\mathbf{n}} \cdot \nabla V)\hat{\mathbf{n}} - \nabla V, \tag{3}$$

where

$$V = c + \hat{\mathbf{n}} \cdot \mathbf{u} \tag{4}$$

is the effective sound speed of the propagating coordinate frame relative to the stationary frame (Lindsay 1960). The Cartesian components for the unit normal to the wavefront (Fig. 2) are given by

$$\hat{\mathbf{n}} = \alpha\hat{\mathbf{1}}_x + \beta\hat{\mathbf{1}}_y + \gamma\hat{\mathbf{1}}_z. \tag{5}$$

The above equations are based on the eikonal equation of geometrical acoustics and WKBJ theory (Goves 1955; Landau & Lifschitz 1951), which is essentially a plane-wave, high-frequency approximation that is satisfied if the fractional variation in the wave amplitude and the change in the ray curvature over the space of a wavelength is small (Tolstoy & Clay 1987; Lindsay 1960). The use of a stratospheric height of 20 km as a wavelength dimension suggests a lower frequency limit of the order of $2 \times 10^{-2}$ Hz for the range of applicability of the geometrical acoustics approach presented herein.

To simplify the application of eqs (1) to (4), we neglect the vertical component and assume negligible horizontal gradients in the atmospheric wind velocity, on the grounds that these are second-order terms. With these assumptions, the horizontal wind velocity is only a function of elevation, $z$,

$$\mathbf{u} = u(z)\hat{\mathbf{1}}_x + v(z)\hat{\mathbf{1}}_y + 0\hat{\mathbf{1}}_z. \tag{6}$$

Expressing eqs (2)–(4) for each Cartesian component, we obtain

$$\dot{x} = \alpha c + u, \qquad \dot{y} = \beta c + v, \qquad \dot{z} = \gamma c, \tag{7a–c}$$

$$V = c + \alpha u + \beta v, \tag{8}$$

$$\dot{\alpha} = \alpha\gamma\frac{\partial V}{\partial z}, \qquad \dot{\beta} = \beta\gamma\frac{\partial V}{\partial z}, \qquad \dot{\gamma} = (\gamma^2 - 1)\frac{\partial V}{\partial z}. \tag{9a–c}$$

From eq. (9)

$$\frac{\dot{\alpha}}{\dot{\beta}} = \frac{\alpha}{\beta} = \text{constant}. \tag{10}$$

Thus, a ray lauched with a horizontal angle $\phi$ measured from the positive $x$-axis (Fig. 2) will retain this angle. The effect of the wind component perpendicular to the direction of the wave normal is to translate the coordinate frame, leaving the ray normal along its original vertical plane. Without any loss of generality, we can align the ray normal along the $x$–$z$ plane, and consider only the ray propagating along that direction. This is equivalent to considering only propagation along a given azimuth. Then $\beta = 0$, and

$$\dot{\alpha} = \alpha\gamma\left(\frac{dc}{dz} + \alpha\frac{du}{dz}\right). \tag{11}$$

Dividing eq. (11) by eq. (7c), we obtain

$$\frac{d\alpha}{dz} = \frac{\alpha^2}{c}\left(\frac{1}{\alpha}\frac{dc}{dz} + \frac{du}{dz}\right). \tag{12}$$

Eq. (12) can be rewritten as

$$\frac{d}{dz}\left(\frac{1}{p}\right) = \frac{d}{dz}\left(\frac{c}{\alpha} + u\right) = 0. \tag{13}$$

The ray parameter, $p$, in a stationary coordinate frame is defined as $p = \alpha/c$, and is conserved along the propagation path. Thus, by redefining $p$ for rays propagating in a moving medium,

$$p = \frac{\alpha}{c}\left(1 + \alpha\frac{u}{c}\right)^{-1}, \tag{14}$$

the ray parameter is conserved along the ray path, in analogy with the windless case. The ray parameter is the inverse of the apparent phase velocity, or trace velocity, and may be identified in array data from $f$–$k$ analysis. To compute the traveltime $T$, the range along the launch azimuth $X$, and the transverse offset $Y$ traversed by a ray, use eqs (7a–c) to obtain

$$\frac{dT}{dz} = \frac{1}{\gamma c}, \tag{15}$$

$$\frac{dX}{dz} = \frac{\alpha c + u}{\gamma c}, \tag{16}$$

$$\frac{dY}{dz} = \frac{v}{\gamma c}. \tag{17}$$

Define the launch angle $\theta$ (Fig. 2), measured from the vertical, so that the horizontal and vertical components of the wave normal are expressed as

$$\alpha = \sin\theta, \tag{18}$$

$$\gamma = \cos\theta = \sqrt{1-\alpha^2}. \tag{19}$$

From eq. (14)

$$\alpha = \frac{pc}{1-pu}. \tag{20}$$

Let $s = c^{-1}$ be the slowness. Then, for a given ray parameter

$$p = \frac{\sin\theta}{c}\left(1+\frac{u\sin\theta}{c}\right)^{-1}, \tag{21}$$

the traveltime, $T$, range along the ray direction, $X$, and transverse offset, $Y$, of a propagating wave over a ray path are

$$T = \int_C s^2\left[s^2 - \frac{p^2}{(1-pu)^2}\right]^{-1/2} dz, \tag{22}$$

$$X = \int_C \left[\frac{p}{(1-pu)} + s^2 u\right]\left[s^2 - \frac{p^2}{(1-pu)^2}\right]^{-1/2} dz, \tag{23}$$

$$Y = \int_C (s^2 v)\left[s^2 - \frac{p^2}{(1-pu)^2}\right]^{-1/2} dz, \tag{24}$$

where the integral is over the vertical distance travelled by the ray path.

It is easy to verify that the above equations reduce to their standard forms when the wind velocity vanishes. Note that, for typical values of the atmospheric winds,

$$|pu| < \left|\frac{u}{c}\right| = M < 1, \tag{25}$$

where $M$ is the Mach number of the wind flow.

As in the windless case, we can use the Legendre transformation (Buland & Chapman 1983) to define the intercept time, $\tau$, as

$$\tau = T - pX, \tag{26}$$

then

$$\tau = \oint (1-pu)\left[s^2 - \frac{p^2}{(1-pu)^2}\right]^{1/2} dz. \tag{27}$$

The tau ($\tau$) function emerges from the variational method of classical mechanics, in the specific case where we seek to minimize the total traveltime $T$ along a wave's propagation path. By applying the Legendre transform (Goldstein 1980), we obtain $\tau$ as our Hamiltonian, with the ray parameter, $p$, acting as a generalized momentum. The tau function is a monotonic function of the ray parameter and does not exhibit the square-root singularities that $X$, $Y$ and $T$ show in eqs (22) and (23). Thus, for a specific traveltime branch, we can construct an interpolation function for tau up to its turning point, and transform tau into a continuous function of the ray parameter (Buland & Chapman 1983). Then, the range for a specific ray parameter (or launch angle), $p_k$, can be obtained from

$$\left.\frac{d\tau}{dp}\right|_{p_k} = -X_k, \tag{28}$$

and the traveltime for a specific arrival at a given range from

$$T_k = \tau(p_k) + p_k X_k. \tag{29}$$

## MODEL RESULTS

To apply eqs (21)–(29), we assume constant-velocity layers and discretize the ray parameter, $p$. The discrete versions of eqs (22)–(24) and eq. (27) are

$$T_{ij} = s_i^2\left[s_i^2 - \frac{p_j^2}{(1-p_j u_i)^2}\right]^{-1/2}\Delta z_i, \tag{30}$$

$$X_{ij} = \left[\frac{p_j}{(1-p_j u_i)} + s_i^2 u_i\right]\left[s_i^2 - \frac{p_j^2}{(1-p_j u_i)^2}\right]^{-1/2}\Delta z_i, \tag{31}$$

$$Y_{ij} = (s_i^2 v_i)\left[s_i^2 - \frac{p_j^2}{(1-p_j u_i)^2}\right]^{-1/2}\Delta z_i, \tag{32}$$

$$\tau_{ij} = (1-p_j u_i)\left[s_i^2 - \frac{p_j^2}{(1-p_j u_i)^2}\right]^{1/2}\Delta z_i, \tag{33}$$

where $i$ denotes the index of the layer at elevation $z_i$, $\Delta z_i = z_{i+1} - z_i$, and $j$ is the index of the discretized ray parameter, $p = \{p_j\}$. Assuming a source at an elevation $z_0$, for each ray parameter we can identify a launch angle, $\theta_0$, measured from the vertical, and given by eq. (20):

$$\theta_0 = \sin^{-1}[pc_0(1-pu_0)^{-1}], \tag{34}$$

where $c_0$ is the sound speed and $u_0$ the wind velocity along the ray path at the source. For the purposes of illustration, in this paper we will consider the case of a source at the Earth's surface, were the winds are assumed to be negligible. However, the method presented here can be applied to a source located anywhere in the atmosphere, with finite winds in the source region. In this case, account is taken of upwards- and downward-propagating branches, as is done in the seismic problem of traveltime determinations (Buland & Chapman 1983).

Fig. 3 shows the real part of tau ($\tau$) as a function of launch angle and elevation for a windless atmosphere and a surface

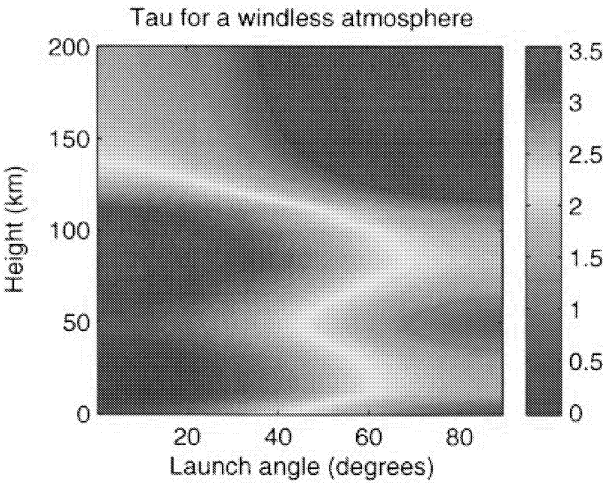


**Figure 3.** Tau for a windless atmosphere as a function of launch angle, measured in degrees from the vertical, and elevation, measured in kilometers.

source, and Fig. 4 shows tau for the same surface source but with the addition of winds for rays propagating north, south, east, and west (Figs 4a–d, respectively). The sound speed and horizontal wind components used as propagation model parameters to compute these two figures are shown in Fig. 1. It is simple to construct any intermediate directions by rotating the wind vector along the desired azimuth. Figs 3 and 4 show that the high-velocity regions map as low-tau regions. As seen in the marked contrast between Figs 3 and 4, the wind introduces significant anisotropy into the propagation medium. The zones where the real part of tau vanishes correspond to turning points for the rays, as can be verified by substituting $p = s_T/(1 + s_T u_T)$ (eq. 21) into eqs (30)–(33), where $s_T$ is the slowness and $u_T$ the wind speed, respectively, at the turning layer.

As seen in Fig. 4, the high-velocity regions in the stratopause and the thermosphere refract acoustic energy that will be ducted between these two high-velocity regions and the Earth's surface. Thermosphere ducted waves and stratopause ducted waves have been recognized by ReVelle & Whitaker (1996) as wave types that are reliably observed at long ranges after large, near-surface explosions. In addition to these two wave types, the authors observed tropopause ducted waves and Lamb waves. The topopause ducted waves correspond to the thin dark zones at high ray parameter and low altitude in Figs 5(b) and (c). These types of guided waves depend strongly on the tropospheric wind field, which may be highly variable. The Lamb wave is a surface-guided wave, and may be implemented into the traveltime computations by defining its propagation velocity and its propagation path. This approach is used in computing arrival times for interface and diffracted waves in the Earth's interior (Buland & Chapman 1983).

By searching for the first turning point for each ray parameter in the tau plots, we define the contributions from the vertical layers for each ray that returns back to the ground. The total traveltime ($T$), range ($X$), transverse offset ($Y$), and tau ($\tau$) as a function of ray parameter for the first skip of waves propagating north are shown in Figs 5 (a)–(d), respectively. As seen in this figure, $T$, $X$, and $Y$ are complicated functions of the ray parameter, and they have four distinct regions which

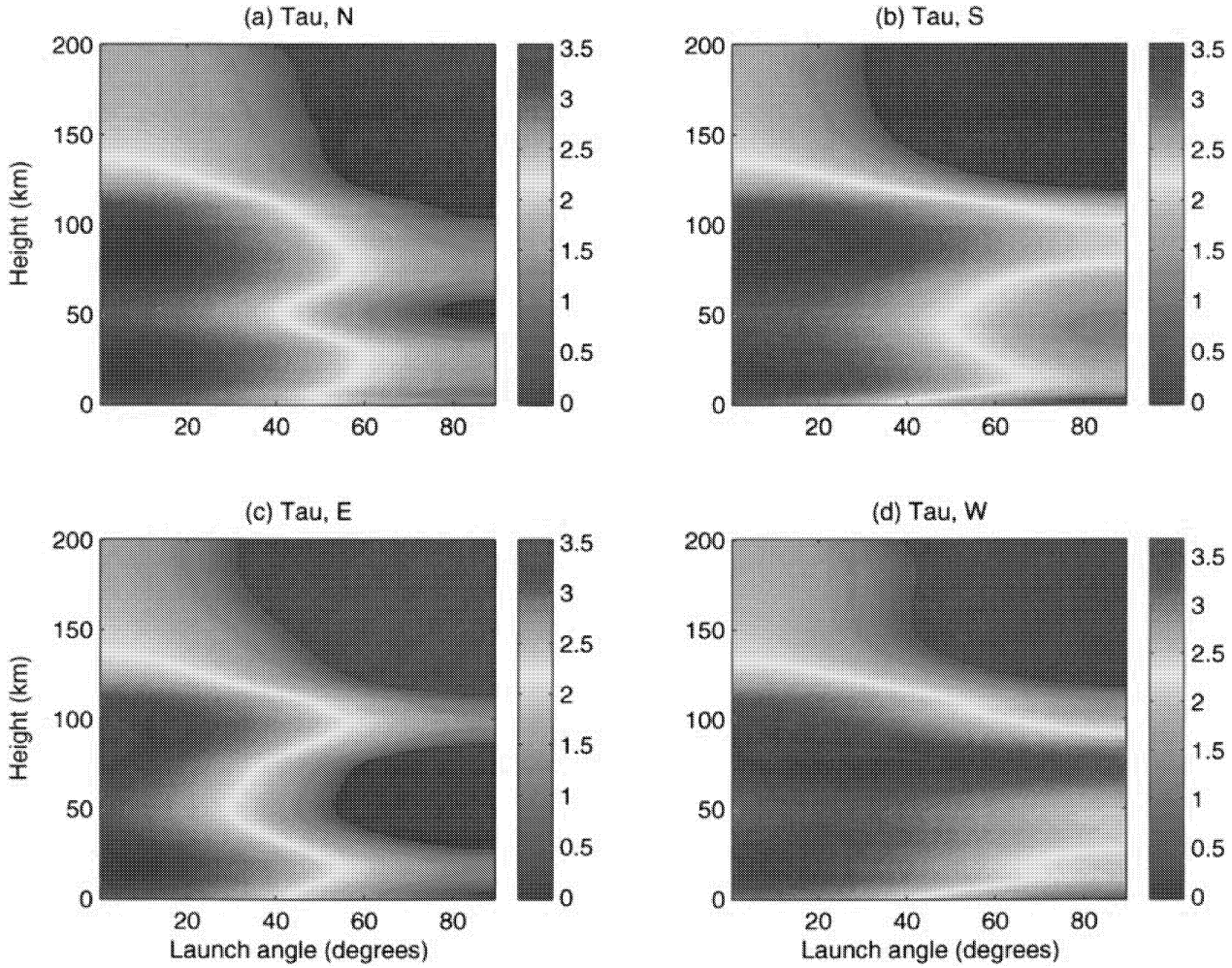


**Figure 4.** Tau as a function of ray parameter and altitude for rays launched towards the (a) north, (b) south, (c) east, and (d) west. Comparison with Fig. 2 shows that there is a significant amount of anisotropy introduced by the wind. Deep blue regions demarcate zones where there are no propagating rays.

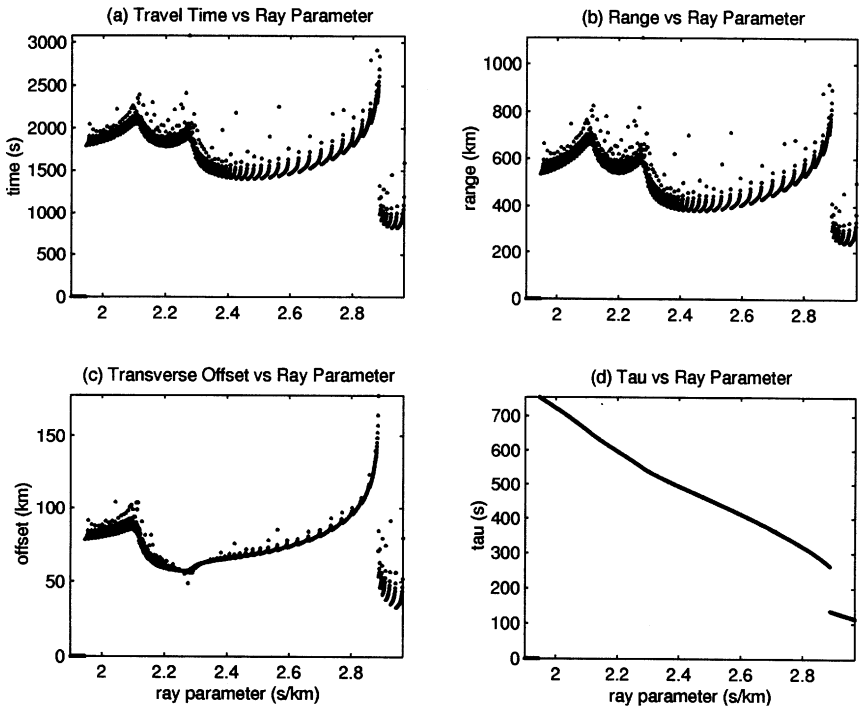


**Figure 5.** (a) Traveltime, (b) range along the ray propagation direction, (c) transverse offset, and (d) tau as a function of ray parameter for waves propagating northwards. Tau is a monotonic function of ray parameter, and shows the transition to new branches as changes in slope.

show concave-upwards curvature. Curves in Figs 5 (a)–(c) corresponding to values of the ray parameter greater than 2.85 s km$^{-1}$ represent launch angles close to the horizontal and refracted at the stratopause and tropopause. The next three branches, at lower ray parameters, are all refracted at the thermosphere, but correspond to different inflections in the ray paths, as can be inferred from Fig. 4(a). In contrast to Figs 5(a)–(c), tau in Fig. 5(d) is a monotonic function of ray parameter, and shows the four branches as changes in the slope, with the stratopause and tropopause branches exhibiting a discontinuity in the tau curve. It is these well-behaved properties of the tau function that permit its interpolation, as discussed in the previous section.

The path contributions for each turning ray are extracted to produce traveltime curves, which are shown in Fig. 6 for waves propagating north, south, east and west (panels, a–d, respectively). Each panel in Fig. 6 corresponds to a single transmission from the ground to the turning point and back to the ground, and shows the variations in the slopes of each branch. Figs 6(a) and (c) shows the branches corresponding to thermospheric refraction and stratopause refraction, and Fig. 6(c) also shows a tropospheric return caused by westerly winds increasing with height in the thermosphere. Figs 6(b) and (d) lack the stratopause-refracted wave, because the winds in that region blow opposite to the direction of wave propagation, thereby reducing the effective sound speed and the angle of refraction of the rays impinging on that region. However, Fig. 6(b) shows a tropospheric return due to the increasing southward wind with height in the lower thermosphere. The slopes of the traveltime curves can be used to determine the slowness of each branch, which yield the apparent phase velocity of each of the phases. These values can then be compared with trace velocities observed by infrasonic arrays in the field, and used to identify specific branches. It is important to point out that the traveltime curves contain no information on the amplitude of the received signal, so a predicted arrival may in fact not be observed because of a small amplitude in the arriving ray tube.

Figs 7(a)–(d) show the transverse offset for rays launched towards the north, south, east, and west, respectively. In Figs 7(a) and (b), positive values are eastward deflections, and in Figs 7(c) and (d), positive values are northward deflections. From eq. (10), the angle $\phi$ (Fig. 2) of the launched ray with respect to the horizonal does not change, and thus the ray retains its original azimuth heading, although the coordinate frame on which the ray is travelling is displaced transversely due to the cross wind. The azimuth deviation is computed from the inverse tangent of $Y/X$. As shown in Fig. 7, specifically Fig. 7(a), nearby infrasonic arrays can show azimuth fluctuations which may lead to significant errors in the initial locations made by using simple triangulation. The incidence azimuth recorded by infrasonic arrays may point along the initial direction of ray propagation, but because of the transverse offset, this incidence azimuth may no longer be directly traced back to its origin without correction. In the specific case of Fig. 7(a), the azimuth deviation at a range of 600 km will range from 5.7° to 9.5°, depending on which of the two thermospheric branches arrive 1800 to 2000 s after an explosion (Fig. 6a). However, if a 90 s window length is used for computing the azimuth and trace velocity perceived by an infrasonic array, an average value of 7.6° may be estimated for the azimuth deviation, and the two distinct branches may not be discernible.

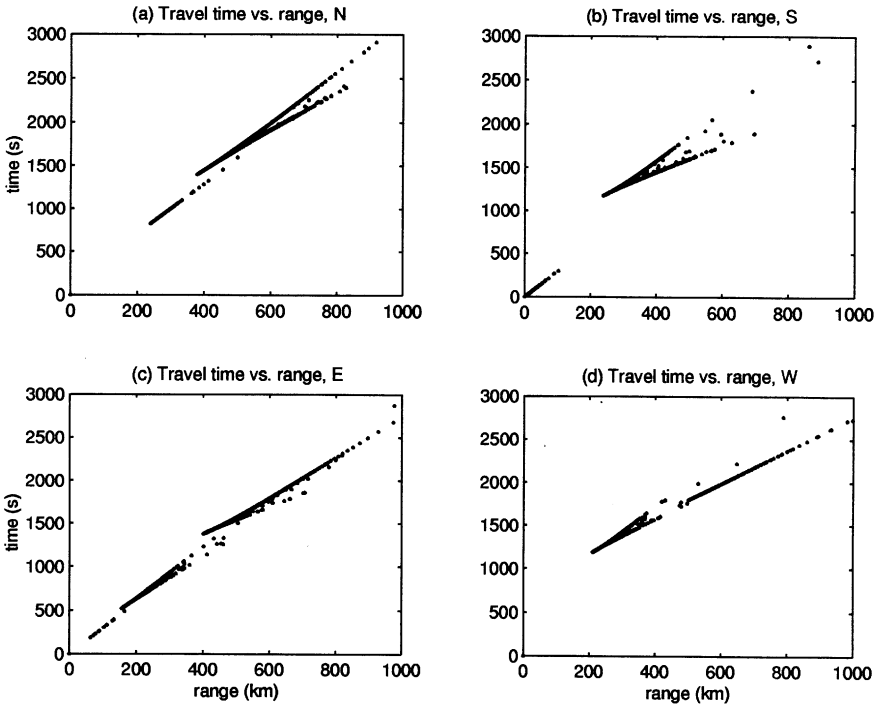


**Figure 6.** Traveltime versus range for rays from a surface source launched towards the (a) north, (b) south, (c) east, and (d) west, computed using the matrices shown in Fig. 3. Propagating branches were calculated by extracting the contributions only up to the first turning point, as seen from the Earth's surface.

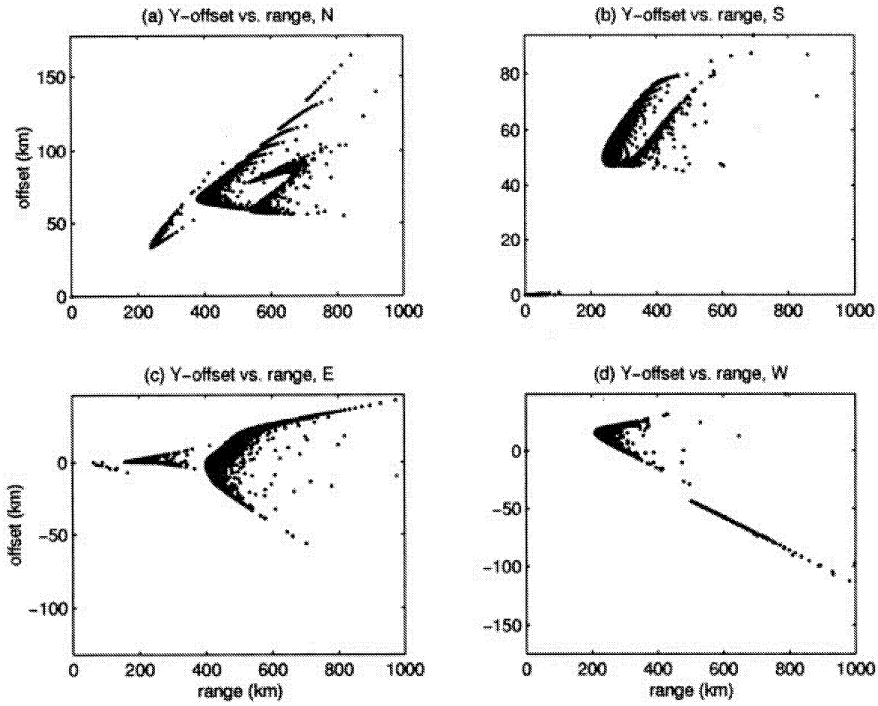


**Figure 7.** Transverse offsets versus range for a surface source launched towards the (a) north, (b) south, (c) east, and (d) west. In panels (a) and (b), positive values correspond to eastward migration; in panels (c) and (d), positive values correspond to northward migration.

Multiple skips of these branches can be easily obtained by adding integer multiples of the travel paths. Thus the range, traveltimes, tau, and transverse offsets of the second bounce are twice those of the first, and the *n*th skip will have *n* times the values of the first bounce. The effect of multiple reflections is to spread out the traveltime curves, so that at long ranges a specific branch will subtend a large horizonal distance, and multiple skips of the same branch will arrive at the same location at different times. However each arrival will possess a distinct ray parameter and azimuth, and it may be possible to identify individual skips if the infrasonic array data are sampled and processed with this application in mind.

As seen in Fig. 6, the first skip of the stratopause and thermosphere ducted waves will travel a distance of approximately 1000 km. Although in principle there is no range limitation to the geometrical acoustics formulation, in practice the overlap of the multiple reflections and refractions from the ground and atmosphere, respectively, may make it difficult to identify individual arrivals past a certain range. A conservative implementation of the tau–*p* method may be restricted to the range delimited by the first three or four skips, which yield an effective range of the order of 3000–4000 km. Using an average Earth radius of 6371 km, this range corresponds to a circle on the spherical Earth with a half-angle of approximately 30°, centred on an infrasonic array. Thus, the implementation of the tau–*p* method in a windy atmosphere may be most effective for frequencies above $2 \times 10^{-2}$ Hz and ranges within a 60° circle centred on the receiving station. For lower frequencies, a normal-mode approach may be more accurate, as in the case of sound propagation in deep water (Tolstoy & Clay 1987). With the range constraint, wind and temperature data need only be averaged in the region overlying each infrasonic station. This will permit more precise atmospheric models and decrease data storage requirements, leading to faster and more accurate determinations of the source location.

To fully implement the tau–*p* method in the field of infrasonics, it is necessary to develop an efficient interpolation scheme to convert tau into a continuous function of ray parameter, and to identify specific propagating branches that can be recognized in the data recorded by infrasonic arrays and used for source location. The success of the traveltime algorithms in infrasonic source detection will pivot on the access to temperature and wind data up to 200 km for regions of interest overlying infrasonic stations, and may demand new signal processing procedures in the monitoring of infrasonic signals.

## CONCLUDING REMARKS

The theoretical framework discussed in this manuscript provides an algorithm for the fast computation of traveltime curves that can be used for the location of sources of infrasonic wave energy. In principle, the formulation presented herein can be applied to range-dependent environments by following the coordinates of a ray as it propagates through each layer and accessing the most recent wind and temperature data for that layer at that location to compute the next set of path contributions. However, the formulation as it is presented in this manuscript is intended for rapid computation, which may be achieved by averaging over the range for a particular azimuth. This approach is a natural extension of the tau–*p* method of Buland & Chapman (1983), and may be used in parallel with seismic wave location algorithms for the determination of wave energy sources in both the solid Earth and the atmosphere. The computer implementation of the algorithm presented in this manuscript is the subject of pilot studies performed at the University of Alaska, Fairbanks, by the authors. Preliminary work on the determination of arrival times for the 1980 October 16 Lop Nor atmospheric nuclear test (Garcés, Lindquist & Hansen 1996) and for the airblast generated by the 1990 destruction of SS-20 missiles in Russia (Garcés & Kulichkov 1997) yielded results consistent with observed infrasonic signals. A functional implementation of the tau–*p* algorithm in the atmosphere will have to access a source of reliable temperature and wind velocity data for the atmosphere up to elevations of 200 km.

## ACKNOWLEDGMENTS

The authors are grateful to D. ReVelle of Los Alamos National Laboratories for his introduction to Lindsay's work and for many helpful discussions, and to D. Clauter at AFTAC for his interest in traveltime determinations and his involvement in global meteorological data sources. Many thanks to J. Tilley, K. Dean, and P. Olsson at the Geophysical Institute, UAF, for their improvements to the original text, and to C. Wilson for providing infrasonic data for the preliminary work. We greatly appreciated valuable revisions from R. Blandford, AFTAC, and from one anonymous reviewer.

## REFERENCES

Beer, T., 1975. *Atmospheric Waves,* Adam Hilger, London.

Buland, R. & Chapman, C., 1983. The computation of seismic travel times, *Bull. seism. Soc. Am.,* **73,** 1271–1302.

Cox, E.F., 1957. Sound propagation in air, in *Handbuch der Physik,* vol. XLVIII, pp. 455–478, eds Bartels, J., Springer-Verlag, Berlin.

Cramer, O., 1992. The variation of the specific ratio and the speed of sound in air with temperature, pressure, humidity, and $CO_2$ concentration, *J. acoust. Soc. Am.,* **93,** 2510–2519.

Diamond, M., 1963. Sound Channels in the atmosphere, *J. geophys. Res.,* **68,** 3459–3464.

Donn, W. & Rind, D., 1971. Natural infrasound as atmospheric probe, *Geophys. J. R. astr. Soc.,* **26,** 111–133.

Fleming, E.L., Chandra, S.H., Burrage, M.D., Skinner, W.R., Hays, P.B., Solheim, B.H. & Sheperd, G.G., 1996. Climatological mean wind observations from the UARS high-resolution Doppler imager and wind imaging interferometer: Comparison with current reference models, *J. geophys. Res.,* **101,** 10 455–10 473.

Garcés, M.A. & Kulichkov, S.N., 1997. Travel times for infrasonic waves in the atmosphere, *Abstracts Infrasound Workshop for CTBT Monitoring,* p. 20, Los Alamos National Laboratory, Santa Fe, NM.

Garcés, M.A., Lindquist, K.G. & Hansen, R.A., 1996. Arrival times for infrasonic waves propagating in a stratified atmosphere, *EOS, Trans. Am. geophys. Un.,* **77,** 115.

Georges, T.M. & Beasley, W.H., 1977. Refraction of infrasound by upper-atmospheric winds, *J. acoust. Soc. Am.,* **61,** 28–34.

Goldstein, H., 1980. *Classical Mechanics,* Addison-Wesley, Reading, MA.

Groves, G.V., 1955. Geometrical theory of sound propagation in the atmosphere, *J. atmos. Terr. Phys.,* **7,** 113–127.

Hedin, A.E., Fleming, E.L., Manson, A.H., Scmidlin, F.J., Avery, S.K., Clark, R.R., Franke, S.J., Fraser, G.J., Tsunda, T., Vial, F. & Vincent, R.A., 1996. Emperical wind model for the upper, middle, and lower atmosphere, *J. atmos. Terr. Phys.,* **58,** 1421–1447.

Hervig, M.E. *et al.,* 1996. Validation of temperature measurements from the Halogen Occultation Experiment, *J. geophys. Res.,* **101,** 10 277–10 285.

Houghton, J.T., 1986. *The Physics of Atmospheres,* Cambridge University Press, Cambridge.

Landau, L.D. & Lifschitz, E., 1951. *Classical Theory of Fields,* Addison-Wesley, Cambridge.

Lindsay, R.B., 1960. *Mechanical Radiation,* McGraw-Hill, New York.

ReVelle, D.O. & Whitaker, R.W., 1996. Lamb waves from airborne explosions sources: viscous effects and comparisons to ducted acoustic arrivals, *Los Alamos National Laboratoires report,* LA-UR-96-3594, New Mexico.

Tolstoy, I. & Clay, C.S., 1987. *Underwater Acoustics. Theory and Experiment in Underwater Sound,* American Institute of Physics, New York.